Inorganic Chemistry
Article
pubs.acs.org/IC

Protonation and Complexation Properties of Polyaromatic Terdentate Six-Membered Chelate Ligands

Thi Nhu Y Hoang,[†] Timothée Lathion,[†] Laure Guénée,[‡] Emmanuel Terazzi,[†] and Claude Piguet*[,†]

[†]Department of Inorganic, Analytical and Applied Chemistry, University of Geneva, 30 quai E. Ansermet, CH-1211 Geneva 4, Switzerland

[‡]Laboratory of Crystallography, University of Geneva, 24 quai E. Ansermet, CH-1211 Geneva 4, Switzerland

Supporting Information

ABSTRACT: The successive protonation steps occurring in 2,2′;6′,2″-terpyridine (**L1**) are characterized by a strong affinity for the first entering proton ($\Delta G^{\mathrm{H,L1}}_{\mathrm{connect}}$ = −17 kJ/mol) followed by allosteric anticooperativity ($\Delta E^{\mathrm{H,H,L1}}_{\mathrm{interaction}}$ = 6 kJ/mol), a behavior mirrored by 2,6-bis(azaindolyl)pyridine (**L2**) despite the extension of the chelate ring size from five members (**L1**) to six members (**L2**; $\Delta G^{\mathrm{H,L2}}_{\mathrm{connect}}$ = −28 kJ/mol and $\Delta E^{\mathrm{H,H,L2}}_{\mathrm{interaction}}$ = 7 kJ/mol). On the contrary, 2,6-bis(8-quinolinyl)pyridine (**L3**) is less eager for the initial protonation ($\Delta G^{\mathrm{H,L3}}_{\mathrm{connect}}$ = −10 kJ/mol), but the fixation of a second proton in $[\mathrm{H_2}\mathbf{L3}]^{2+}$ is driven to completion by positive cooperativity ($\Delta E^{\mathrm{H,H,L3}}_{\mathrm{interaction}}$ = −5 kJ/mol). Because of its unusual ability to adopt a cis–cis conformation with a large affinity for the entering protons, **L2** has been selected for exploring the reactivity of a terdentate fused six-membered chelate with labile metallic cations possessing increasing electrostatic factors along the series M^{z+} = Li^+ < Mg^{2+} ≈ Zn^{2+} < Y^{3+}. Spectroscopic, thermodynamic, and structural studies demonstrate that covalency is crucial for stabilizing the complexes $[\mathrm{Zn}(\mathbf{L2})_n]^{2+}$. With the highly charged Y^{3+} cation, hydrolysis drastically competes with ligand complexation, but anhydrous conditions restore sufficient selectivity for the successful coordination of neutral fused six-membered polyaromatic terdentate chelates with large 4f-block cations.

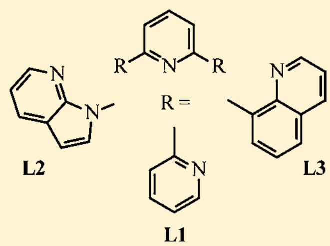

INTRODUCTION

The origin of the systematic preference of large p- and d-block cations for five-membered chelate rings over six-, seven-, or eight-membered analogues has been the subject of intense activity during the late 1980s.[1] Taking cyclopentane and cyclohexane as structural models for these metallocycles, molecular mechanics predicts that only five-membered chelate rings adopt a low strain geometry around a large M^{2+} cation, whereas six-membered rings require too short M-donor bonds (~1.54 Å) and too large bite angles (~109.5°; Scheme 1).[1] When additional structural constraints are introduced through the incorporation of rigid aromatic units within the chelate ring, the pertinence of this simple analysis becomes debatable, and large trivalent lanthanide cations, Ln^{III}, form stable complexes with anionic seven-,[2] six-,[3] and five-membered[4] aromatic chelate rings (Figure S1 in the Supporting Information, SI).

In this context, neutral N-heterocyclic donor atoms in bidentate 2,2′-bipyridine and terdentate 2,2′;6′,2″-terpyridine (**L1**; Scheme 2) also provide reasonably stable five-membered chelate complexes with Ln^{III}.[5,6] Surprisingly, the extended

Scheme 1. Lowest Strain Energy Geometry Calculated Using Molecular Mechanics for (a) a Five-Membered Chelate Ring and (b) a Six-Membered Chelate Ring Adapted from reference 1b

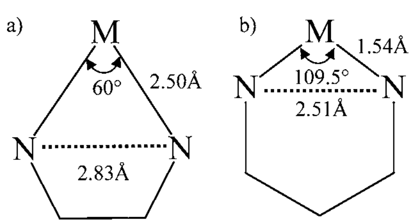

Scheme 2. Chemical Structures of the Terdentate Ligands L1−L3 with Numbering Schemes for NMR Studies

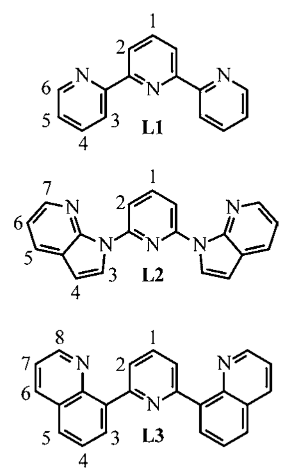

Received: May 29, 2012
Published: July 19, 2012

   dx.doi.org/10.1021/ic301126y | Inorg. Chem. 2012, 51, 8567−8575

analogous six-membered chelates 2,6-bis(azaindolyl)pyridine (**L2**)[7] and 2,6-bis(8-quinolinyl)pyridine (**L3**)[8] have not been considered for the coordination of Ln^{III}, while some complexes with d-block cations of variable sizes such as Mn^{II} (67 pm),[9] Cu^{II} (73 pm),[10] Ru^{II} (>82 pm),[11] and Pt^{II} (94 pm)[12] have been isolated and characterized in the solid state.

As expected, titration of **L1** with $Eu(CF_3SO_3)_3 \cdot H_2O$ in $CD_3CN/CDCl_3$ (1:1) displays the successive formation of $[Eu(\mathbf{L1})_2S_3]^{3+}$ and $[Eu(\mathbf{L1})S_6]^{3+}$ (S = solvent molecule) characterized by their paramagnetically shifted ^{1}H NMR signals (Figure S2a in the SI).[6a] In these complexes, each terpyridine ligand **L1** is meridionally tercoordinated to Ln^{III}, thus producing two fused five-membered chelate rings.[6] Repeating these titrations with the six-membered chelating ligands **L2** (Figure S2b in the SI) and **L3** (Figure S2c in the SI) shows no trace of paramagnetic effects, but the detection of exchange-broadened spectra on the NMR time scale, which are diagnostic for the formation of the monoprotonated species $[H\mathbf{L2}]^+$ and $[H\mathbf{L3}]^+$ (vide infra). Equilibria (1)−(3) correspond to a simple model rationalizing these observations.

$$Eu^{3+} + H_2O \rightleftharpoons [Eu(OH)]^{2+} + H^+ \qquad K_a^1 \tag{1}$$

$$Eu^{3+} + \mathbf{L}\boldsymbol{k} \rightleftharpoons [Eu(\mathbf{L}\boldsymbol{k})]^{3+} \qquad \beta_{1,0,1}^{Eu,H,\mathbf{L}\boldsymbol{k}} \tag{2}$$

$$H^+ + \mathbf{L}\boldsymbol{k} \rightleftharpoons [H\mathbf{L}\boldsymbol{k}]^+ \qquad \beta_{0,1,1}^{Eu,H,\mathbf{L}\boldsymbol{k}} \tag{3}$$

Once K_a^1 is at hand ($K_a^1 = 10^{-8.81}$ in a 0.3 M $NaClO_4$ aqueous solution),[13] the competition between ligand complexation (eq 2) and ligand protonation (eq 3) is estimated by the concentration ratio $|[Eu(\mathbf{L}\boldsymbol{k})]^{3+}|/|[H\mathbf{L}\boldsymbol{k}]^+|$ given in eq 4 (see Appendix 1 in the SI).

$$\frac{|[Eu(\mathbf{L}\boldsymbol{k})^{3+}]|}{|[H\mathbf{L}\boldsymbol{k}^+]|} = \frac{\beta_{1,0,1}^{Eu,H,\mathbf{L}\boldsymbol{k}}}{\beta_{0,1,1}^{Eu,H,\mathbf{L}\boldsymbol{k}}} \frac{(|H_2O|_{tot} - |H_2O|)}{K_a^1|H_2O|} \tag{4}$$

The exclusive ^{1}H NMR detection of $[Eu(\mathbf{L1})]^{3+}$ under stochiometric conditions ($|[Eu(\mathbf{L}\boldsymbol{k})]^{3+}|/|[H\mathbf{L}\boldsymbol{k}]^+| \geq 100$; Figure S2a in the SI) contrasts with the quantitative formation of $[H\mathbf{L}\boldsymbol{k}]^+$ for **L2** and **L3** in the same conditions ($|[Eu(\mathbf{L}\boldsymbol{k})]^{3+}|/|[H\mathbf{L}\boldsymbol{k}]^+| \leq 0.01$; Figure S2b,c in the SI). This implies that $\beta_{1,0,1}^{Eu,H,\mathbf{L}\boldsymbol{k}}/\beta_{0,1,1}^{Eu,H,\mathbf{L}\boldsymbol{k}}$ drastically decreases for the six-membered chelating ligands **L2** and **L3**, but there is no way to point out the exact influence of each individual contribution (protonation and complexation). Therefore, we first report here on the thermodynamics of the protonation reactions of **L1**−**L3** in $CD_3CN/CDCl_3$, which control the denominator of eq 4. The six-membered chelating ligand with the largest proton affinity ($\beta_{0,1,1}^{M,H,\mathbf{L}\boldsymbol{k}} = \beta_{1,1}^{H,\mathbf{L}\boldsymbol{k}}$) is then investigated for its potential complexation properties with labile transition-metal cations, which maximize the numerator of eq 4 (i.e., $\beta_{1,0,1}^{M,H,\mathbf{L}\boldsymbol{k}}$) in organic solvents.

■ RESULTS AND DISCUSSION

Protonation of Ligands L1−L3. **L1** is known to bind two successive protons according to equilibria (5) and (6) in water [$\log(\beta_{1,1}^{H,\mathbf{L1}})$ = 4.32(3) and $\log(\beta_{1,2}^{H,\mathbf{L1}})$ = 7.59(4)][14] and in aqueous organic solvents.[15]

$$H^+ + \mathbf{L}\boldsymbol{k} \rightleftharpoons [H\mathbf{L}\boldsymbol{k}]^+ \qquad \beta_{1,1}^{H,\mathbf{L}\boldsymbol{k}} \tag{5}$$

$$2H^+ + \mathbf{L}\boldsymbol{k} \rightleftharpoons [H_2\mathbf{L}\boldsymbol{k}]^{2+} \qquad \beta_{2,1}^{H,\mathbf{L}\boldsymbol{k}} \tag{6}$$

^{1}H NMR titrations of **L1** in $CD_3CN/CDCl_3$ (1:1) with CF_3SO_3H exhibit fast-exchange processes on the NMR time scale (Figure S3 in the SI), and the complete set of weight-average chemical shifts can be satisfyingly fitted to equilibria (5) and (6) by using nonlinear least-squares techniques to give $\log(\beta_{1,1}^{H,\mathbf{L1}})$ = 3.4(1) and $\log(\beta_{1,2}^{H,\mathbf{L1}})$ = 5.2(1) (Table 1).

Table 1. Cumulative Thermodynamic Protonation Constants [$\log(\beta_{m,1}^{H,\mathbf{L}\boldsymbol{k}})$], Associated Microscopic Affinities [$\log(f_{connect}^{H,\mathbf{L}\boldsymbol{k}})$ and $\Delta G_{connect}^{H,\mathbf{L}\boldsymbol{k}}$], Intramolecular Interproton Interactions [$\log(u_{\mathbf{L}\boldsymbol{k}}^{H,H})$ and $\Delta G_{interaction}^{H,H,\mathbf{L}\boldsymbol{k}}$], and Allosteric Cooperativity Factors (α)^a Obtained by ^{1}H NMR Titrations of L1−L3 with CF_3SO_3H in $CD_3CN/CDCl_3$ (1:1) at 298 K

	L1	L2	L3
$\log(\beta_{1,1}^{H,\mathbf{L}\boldsymbol{k}})$	3.4(1)	5.3(3)	2.3(2)
$\log(\beta_{2,1}^{H,\mathbf{L}\boldsymbol{k}})$	5.2(1)	8.9(3)	5.0(1)
$\log(f_{connect}^{H,\mathbf{L}\boldsymbol{k}})$	2.9(1)	4.8(3)	1.8(2)
$\Delta G_{connect}^{H,\mathbf{L}\boldsymbol{k}}$/(kJ/mol)	−16.7(6)	−27.5(1.7)	−10.4(1.1)
$\log(u_{\mathbf{L}\boldsymbol{k}}^{H,H})$	−1.1(2)	−1.2(5)	0.9(3)
$\Delta E_{interaction}^{H,H,\mathbf{L}\boldsymbol{k}}$/(kJ/mol)	6.4(1.0)	7.0(3.0)	−5.0(1.7)
α^a	0.08(3)	0.06(7)	7.5(5.2)

$^a\alpha = [(\omega_{1,1}^{H,\mathbf{L}\boldsymbol{k}})^2/\omega_{2,1}^{H,\mathbf{L}\boldsymbol{k}}][\beta_{2,1}^{H,\mathbf{L}\boldsymbol{k}}/(\beta_{1,1}^{H,\mathbf{L}\boldsymbol{k}})^2] = 3[\beta_{2,1}^{H,\mathbf{L}\boldsymbol{k}}/(\beta_{1,1}^{H,\mathbf{L}\boldsymbol{k}})^2]$.[28]

Compared with water, the stepwise affinities of **L1** for protons in $CD_3CN/CDCl_3$ are reduced by approximately 1 order of magnitude, which limits the relative quantity of $[H\mathbf{L1}]^+$ and $[H_2\mathbf{L1}]^{2+}$ formed in solution at millimolar concentrations (Figure 1a).

The individual ^{1}H NMR spectra computed for **L1**, $[H\mathbf{L1}]^+$, and $[H_2\mathbf{L1}]^{2+}$ show the systematic downfield shifts of the aromatic protons upon successive protonation (Figure 1b), a trend resulting from a decrease in the electronic density brought on by the protonation of N-heterocyclic aromatic rings in $[H\mathbf{L1}]^+$ and $[H_2\mathbf{L1}]^{2+}$.[17] Interestingly, the local magnetic environments of the protons H2 and H3 are further sensitive to the cisoid versus transoid conformations adopted by the terdentate ligand (Scheme 3). The abnormal zigzag behavior observed for H3 ($\Delta\delta$ = 0.45 ppm on going from **L1** to $[H\mathbf{L1}]^+$ and $\Delta\delta$ = −0.97 ppm on going from $[H\mathbf{L1}]^+$ to $[H_2\mathbf{L1}]^{2+}$; Figure 1b) is diagnostic for the initial protonation of trans−trans terpyridine **L1** (Scheme 3, top)[18,19] onto one distal pyridine ring to give $[H\mathbf{L1}]^+$, which exists in solution as fast-interconverting cis−trans C_s-symmetrical conformers (Scheme 3, middle),[20] followed by the connection of a second proton to give the average coplanar cis−cis isomer in $[H_2\mathbf{L1}]^{2+}$ (the H3 protons are no more affected by the electronegative nitrogen atoms of the central pyridine ring; Scheme 3, bottom).[21] This sequence of protonation steps and conformational changes agrees with the molecular structures reported for **L1**,[18] $[H\mathbf{L1}]^+$,[20] and $[H_2\mathbf{L1}]^{2+}$ [21] in the solid state (Figure S4 in the SI).

^{1}H NMR titrations with **L2** (Figure S5 in the SI) and **L3** (Figure S6 in the SI) also show the successive fixation of two protons to give $[H\mathbf{L}\boldsymbol{k}]^+$ (eq 5) and $[H_2\mathbf{L}\boldsymbol{k}]^{2+}$ (eq 6, k = 2, 3), from which $\log(\beta_{1,1}^{H,\mathbf{L}\boldsymbol{k}})$ and $\log(\beta_{2,1}^{H,\mathbf{L}\boldsymbol{k}})$ are obtained by nonlinear least-squares fits (Table 1).[16]

Except for a smaller affinity for the connection of the first entering proton, the thermodynamic protonation constants found for **L3** roughly mirror those found for **L1** (Table 1), thus leading to comparable distributions of species in solution (Figures 1a and 2b, top). The stepwise downfield shift of H1 and H6 observed upon protonation of **L3**,[17] combined with the

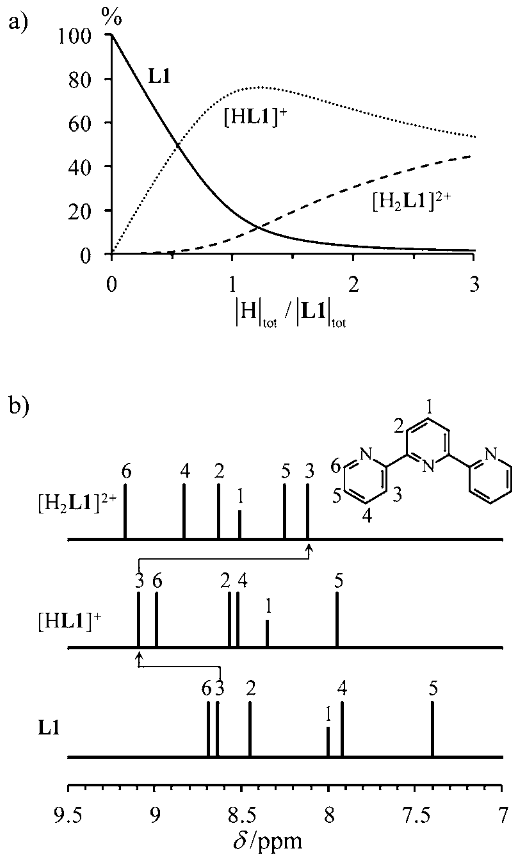

Figure 1. Computed (a) ligand distribution and (b) individual ^{1}H NMR spectra for **L1**, $[H\mathbf{L1}]^+$, and $[H_2\mathbf{L1}]^{2+}$ $[CD_3CN/CDCl_3$ (1:1); total ligand concentration 15 mM; 298 K].

Scheme 3. Possible Dynamically Averaged Conformations Adopted by the Aromatic Tridentate Ligand L1 and Its Protonated Forms $[H\mathbf{L1}]^+$ and $[H_2\mathbf{L1}]^{2+a}$

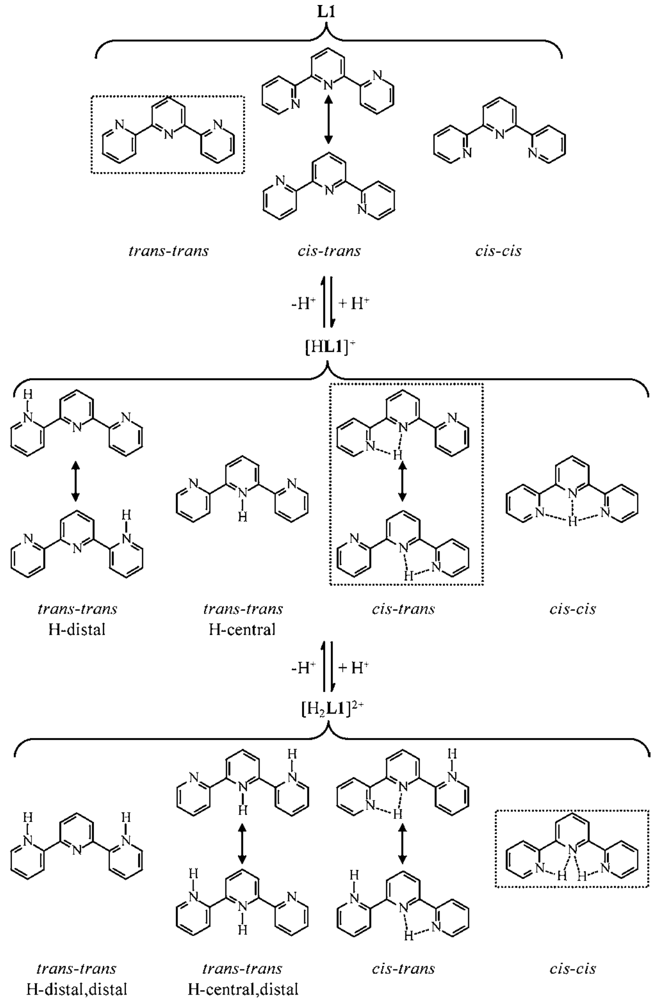

^{a}The conformations observed in the crystal structures and in solution are surrounded.

zigzag behavior of H3 (downfield shift $\Delta\delta = 0.95$ ppm on going from **L3** to $[H\mathbf{L3}]^+$, followed by an upfield shift $\Delta\delta = -0.61$ ppm on going from $[H\mathbf{L3}]^+$ to $[H_2\mathbf{L3}]^{2+}$; Figure 2b, bottom, and Table S1 in the SI) indicate an average cis−trans conformation for $[H\mathbf{L3}]^+$ in solution (as found for $[H\mathbf{L1}]^+$), whereas $[H_2\mathbf{L3}]^{2+}$ adopts the cis−cis conformation (as found for $[H_2\mathbf{L1}]^{2+}$). On the contrary, **L2** binds two successive protons with 2 orders of magnitude larger affinities, thus leading to the successive (almost) quantitative formations of $[H\mathbf{L2}]^+$ and $[H_2\mathbf{L2}]^{2+}$ at stoichiometric ratios for millimolar concentrations (Figure 2a, top). Moreover, the structurally sensitive protons H2 and H3 now exhibit reverse zigzag behaviors (Figure 2a, bottom, and Table S2 in the SI). The initial upfield shifts of H2 and H3 point to the removal of the interaction of these protons with the adjacent nitrogen atoms of the central pyridine ring, as a result of the unusual cis−cis conformation adopted by $[H\mathbf{L2}]^+$. The minor additional shift detected upon the addition of a second proton in $[H_2\mathbf{L2}]^{2+}$ suggests that the latter conformation is retained in the fully protonated ligand.

In line with the lack of measurable inter-ring H···H nuclear Overhauser enhancement (NOE) effects for the unprotonated ligands in solution, the molecular structures of **L1** (Figure S4a, top, in the SI),[18] **L2** (Figure 3a, top),[10] and **L3** (Figure 4a, top)[8] in the solid state systematically show the terdentate ligand strand to adopt the trans−trans conformation, which minimizes both steric constraints and intramolecular electric multipolar interactions.[15,22] Whereas the closest inter-ring interatomic contact distances in **L1** [N(distal)···H(central) = 2.94 Å; Figure S4b, top, in the SI] and in **L2** [N(distal)···H(central) = 2.26 Å; Figure 3b, top] are compatible with an approximate coplanar arrangement of the three aromatic rings, **L3** displays a significant twist (interplanar pyridine−quinoline angles = 46.4−47.0°; Figure 4b top) for restoring an acceptable contact distance N(distal)···H(central) = 2.65 Å.[23] Protonations of **L2** and **L3** with CF_3SO_3H in CH_2Cl_2/CH_3CN (1:1), followed by the slow evaporation or diffusion of diethyl ether yield X-ray-quality prisms for $[H\mathbf{L2}](CF_3SO_3)$ (**1**), $[H_2\mathbf{L2}](CF_3SO_3)_2$ (**2**), $[H\mathbf{L3}](CF_3SO_3)$ (**3**), and $[H_2\mathbf{L3}](CF_3SO_3)_2$ (**4**). Each structure is constituted of protonated cations displaying weak (if any) contacts with ionic triflate counter-anions (Tables S2−S14 and Figures S7−S10 in the SI).[24,25] Similarly to $[H\mathbf{L1}]^+$, the molecular structure of the monoprotonated six-membered analogue $[H\mathbf{L3}]^+$ adopts a pseudo-cis−trans conformation, in which the two rings interacting with the entering proton are coplanar (interplanar pyridine−quinoline angle = 3.4°; Table S10 in the SI and Figure 4, middle). The additional hydrogen atom is located on the nitrogen atom of the central pyridine ring, and it forms a bent hydrogen bond with the nitrogen atom of the adjacent coplanar quinoline ring (Figure 4b, middle, and Figure S8a and

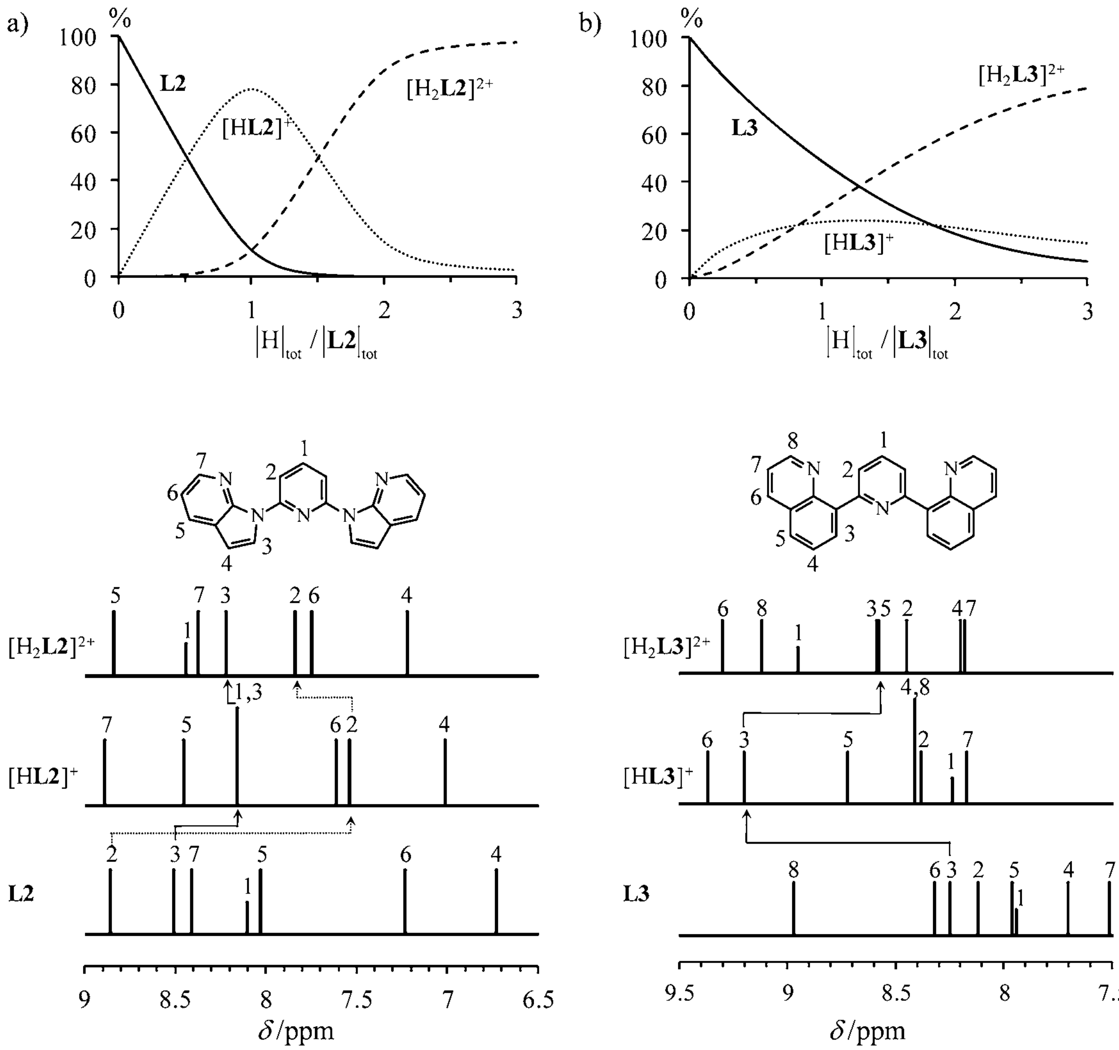

Figure 2. Computed ligand distribution and individual ^{1}H NMR spectra for (a) **L2**, [H**L2**]$^+$, and [H$_2$**L2**]$^{2+}$ and (b) **L3**, [H**L3**]$^+$, and [H$_2$**L3**]$^{2+}$ [CD$_3$CN/CDCl$_3$ (1:1); total ligand concentration 15 mM; 298 K].

Table S11 in the SI). In excess of acid, the two distal quinoline rings are protonated in [H$_2$**L3**]$^{2+}$, which adopts the cis–cis conformation similarly observed for [H$_2$**L1**]$^{2+}$, but twisted along the aromatic backbone (interplanar pyridine–quinoline angles = 23.9–31.6°; Table S13 in the SI and Figure 4, bottom). Two weak and bent intramolecular hydrogen bonds contribute to stabilization of the molecular edifice (Figure 4, bottom, and Table S14 and Figure S8b in the SI). The situation is quite different for [H**L2**]$^+$, because the entering proton is trapped within a cavity of three nitrogen atoms brought by the coplanar cis–cis arrangement of the three aromatic rings (interplanar pyridine–azaindole angles = 3.7–4.2°; Table S4 in the SI and Figure 3, middle). A bifurcated hydrogen bond links the distal N(azaindole)–H donor with the two adjacent nitrogen atoms of the other aromatic rings (Table S5 and Figure S7a in the SI). The fixation of the second proton in [H$_2$**L2**]$^{2+}$ occurs on the second azaindole ring, which produces the usual helical twist of the polyaromatic backbone (interplanar azaindole-pyridine rings = 20.9–31.7°; Table S7 in the SI and Figure 3, bottom) stabilized by weak bent hydrogen bonds (Figure 3, bottom, and Table S8 and Figure S7 in the SI).

We conclude that the solution structures established by ^{1}H NMR fairly agree with the molecular structures observed in the solid state. For **L1** and **L3**, the thermodynamic protonation constants are comparable and the *trans*–*trans*-**L*k*** arrangement found for the nonprotonated ligands transforms into *cis*–*trans*-[H**L*k***]$^+$ and *cis*–*cis*-[H$_2$**L*k***]$^{2+}$. For **L2**, the protonation steps are thermodynamically more favorable because the initial coplanar *trans*–*trans*-**L2** arrangement is transformed into coplanar cis–cis conformations in both [H**L2**]$^+$ and [H$_2$**L2**]$^{2+}$.

Taking the molecular structures of *cis*–*cis*-[H$_2$**L*k***]$^{2+}$ (k = 1–3) as rough models for the meridional tercoordination of these ligands around multivalent cations, the fused polyaromatic five-membered chelate rings in **L1** mainly differ from the fused polyaromatic six-membered chelate rings in **L2** and **L3** by the geometry of the pseudoisosceles triangles drawn by the three nitrogen donor atoms (Figure 5). For each triangle, the nitrogen atom of the central pyridine ring occupies the apex position, but only [H$_2$**L1**]$^{2+}$ possesses an obtuse apex angle, which leads to a flattened arrangement of the three nitrogen donor atoms compatible with the encapsulation of large cations ($d_{\mathrm{N(distal)-N(distal)}}$ = 4.55 Å; Figure 5a). The acute isosceles triangles observed for [H$_2$**L2**]$^{2+}$ and [H$_2$**L3**]$^{2+}$ result in shorter N(distal)···N(distal) contact distances (3.39–3.64 Å; Figure 5b,c), which are expected to be less favorable for the approach of large cations.

dx.doi.org/10.1021/ic301126y | Inorg. Chem. 2012, 51, 8567–8575

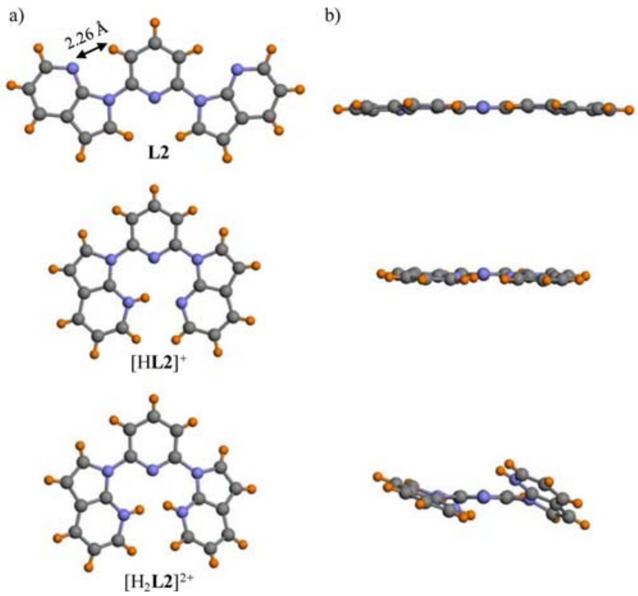

Figure 3. Perspective views (a) perpendicular and (b) parallel to the central pyridine ring of the molecular structures of **L2**, $[H\mathbf{L2}]^+$, and $[H_2\mathbf{L2}]^{2+}$ observed in the crystal structures of **L2**,[10] **1**, and **2**. Color code: gray, C; blue, N; orange, H.

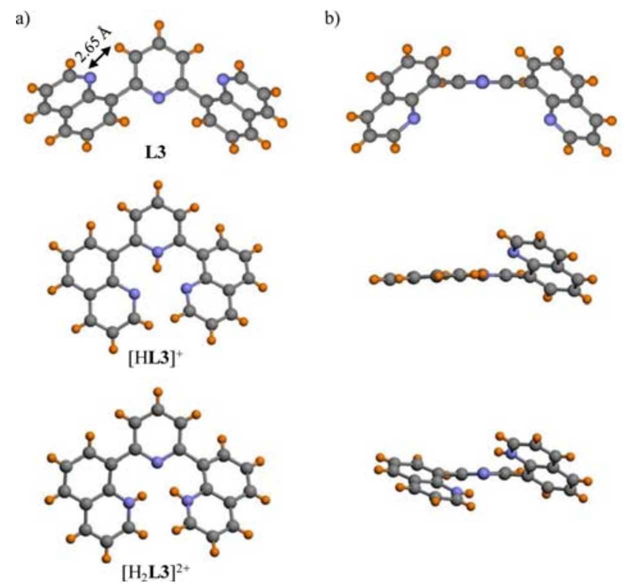

Figure 4. Perspective views (a) perpendicular and (b) parallel to the central pyridine ring of the molecular structures of **L3**, $[H\mathbf{L3}]^+$, and $[H_2\mathbf{L3}]^{2+}$ observed in the crystal structures of **L3**,[8] **3**, and **4**. Color code: gray, C; blue, N; orange, H.

Thermodynamic Modeling for the Protonation Steps in Ligands L1−L3. Within the frame of the site-binding approach,[26] the cumulative protonation constants (eqs 5 and 6) can be modeled with eqs 7 and 8, respectively.

$$\beta_{1,1}^{\mathrm{H},\mathbf{L}k} = \omega_{1,1}^{\mathrm{H},\mathbf{L}k}(\mathrm{distal})\, f_{\mathrm{distal}}^{\mathrm{H},\mathbf{L}k} + \omega_{1,1}^{\mathrm{H},\mathbf{L}k}(\mathrm{central})\, f_{\mathrm{central}}^{\mathrm{H},\mathbf{L}k} \quad (7)$$

$$\beta_{2,1}^{\mathrm{H},\mathbf{L}k} = \omega_{1,1}^{\mathrm{H},\mathbf{L}k}(\mathrm{distal})\, (f_{\mathrm{distal}}^{\mathrm{H},\mathbf{L}k})^2 u_{\mathrm{d,d},\mathbf{L}k}^{\mathrm{H},\mathbf{L}k} + \omega_{2,1}^{\mathrm{H},\mathbf{L}k}(\mathrm{central})\, (f_{\mathrm{central}}^{\mathrm{H},\mathbf{L}k})(f_{\mathrm{distal}}^{\mathrm{H},\mathbf{L}k}) u_{\mathrm{c,d},\mathbf{L}k}^{\mathrm{H,H}} \quad (8)$$

In these equations, $\omega_{n,1}^{\mathrm{H},\mathbf{L}k}$ takes into account the pure statistical (i.e., entropic) contribution due to a change in the molecular rotational entropies occurring upon protonation.[27] Once the point group of each partner contributing to equilibria (5) and (6) is at hand, $\omega_{m,1}^{\mathrm{H},\mathbf{L}k}$ values are easily computed using the method of symmetry numbers (Figures S14 and S15 in the SI).[27] $f_{\mathrm{distal}}^{\mathrm{H},\mathbf{L}k}$ and $f_{\mathrm{central}}^{\mathrm{H},\mathbf{L}k}$ correspond to the absolute affinities of the distal and central heterocyclic aromatic rings, respectively, for its intermolecular connection with a proton. Application of the van't Hoff isotherm transforms these thermodynamic describers into free energies of connection $\Delta G_{\mathrm{distal}}^{\mathrm{H},\mathbf{L}k} = -RT\ln(f_{\mathrm{distal}}^{\mathrm{H},\mathbf{L}k})$ and $\Delta G_{\mathrm{central}}^{\mathrm{H},\mathbf{L}k} = -RT\ln(f_{\mathrm{central}}^{\mathrm{H},\mathbf{L}k})$, which include desolvation processes (the standard concentration of the reference state is set to 1 M).[26d] Finally, $u_{\mathrm{d,d},\mathbf{L}k}^{\mathrm{H,H}} = \exp[-(\Delta E_{\mathrm{d,d},\mathbf{L}k}^{\mathrm{H,H}}/RT]$ and $u_{\mathrm{c,d},\mathbf{L}k}^{\mathrm{H,H}} = \exp[-(\Delta E_{\mathrm{c,d},\mathbf{L}k}^{\mathrm{H,H}}/RT]$ are the Boltzmann factors correcting the free energy of connection for any intramolecular H···H interactions resulting from the close location of the two protons in $[H_2\mathbf{L}k]^{2+}$ (d,d = distal−distal interactions and c,d = central−distal interactions). Taking into account the structural information brought by the combination of ^{1}H NMR and X-ray crystal structures, two averaged coplanar trans−cis conformers contribute to the macrospecies $[H\mathbf{L}k]^+$ in solution (i.e., protonation occurring either on the central or on the distal cis-aromatic rings; Figure S14 in the SI) and two averaged coplanar cis−cis conformers contribute to the macrospecies $[H_2\mathbf{L}k]^{2+}$ (i.e., protonations occurring either on the central−distal or on the distal−distal pair positions of the aromatic rings; Figure S15 in the SI). Consequently, each associated macroconstant in eqs 7 and 8 combines two microconstants, eventually leading to eqs 10 and 11 after the introduction of adequate statistical factors.

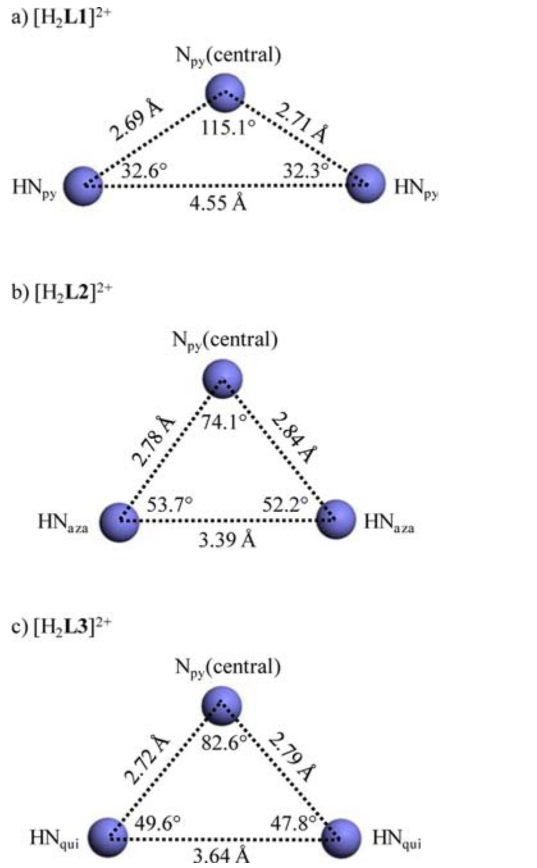

Figure 5. Geometries of the pseudoisosceles triangles formed by the nitrogen donor atoms in the molecular structures of (a) $[H_2\mathbf{L1}]^{2+}$, (b) $[H_2\mathbf{L2}]^{2+}$ and (c) $[H_2\mathbf{L3}]^{2+}$.

$$\beta_{1,1}^{\mathrm{H},\mathbf{L}k} = 2f_{\mathrm{distal}}^{\mathrm{H},\mathbf{L}k} + f_{\mathrm{central}}^{\mathrm{H},\mathbf{L}k} \quad (10)$$

$$\beta_{2,1}^{\mathrm{H},\mathbf{L}k} = \omega_{1,1}^{\mathrm{H},\mathbf{L}k}(\mathrm{distal})\,(f_{\mathrm{distal}}^{\mathrm{H},\mathbf{L}k})^2 u_{\mathrm{d,d},\mathbf{L}k}^{\mathrm{H},\mathbf{L}k} + \omega_{2,1}^{\mathrm{H},\mathbf{L}k}(\mathrm{central})\,(f_{\mathrm{central}}^{\mathrm{H},\mathbf{L}k})(f_{\mathrm{distal}}^{\mathrm{H},\mathbf{L}k})u_{\mathrm{c,d},\mathbf{L}k}^{\mathrm{H,H}} \quad (11)$$

Reasonably assuming for each specific ligand **L***k* that (i) the affinity of the proton for the central and distal aromatic rings are comparable ($f_{\mathrm{distal}}^{\mathrm{H,L}k} \approx f_{\mathrm{central}}^{\mathrm{H,L}k} = f_{\mathrm{connect}}^{\mathrm{H,L}k}$) and (ii) the interproton interactions operating within each microspecies contributing to $[\mathrm{H_2L}k]^{2+}$ are similar $u_{\mathrm{d,d,L}k}^{\mathrm{H,H}} \approx u_{\mathrm{d,d,L}k}^{\mathrm{H,H}} = u_{\mathrm{L}k}^{\mathrm{H,H}}$, eqs 10 and 11 reduce to

$$\beta_{1,1}^{\mathrm{H},\mathbf{L}k} = 3f_{\mathrm{connect}}^{\mathrm{H},\mathbf{L}k} \quad (12)$$

$$\beta_{2,1}^{\mathrm{H},\mathbf{L}k} = 3(f_{\mathrm{connect}}^{\mathrm{H},\mathbf{L}k})^2 u_{\mathbf{L}k}^{\mathrm{H,H}} \quad (13)$$

Introducing the experimental protonation constants $\beta_{1,1}^{\mathrm{H,L}k}$ and $\beta_{2,1}^{\mathrm{H,L}k}$ collected for each ligand (Table 1, entries 1 and 2) into eqs 12 and 13 provides $\log(f_{\mathrm{connect}}^{\mathrm{H,L}k})$ (Table 1, entry 3) and $\log(u_{\mathrm{L}k}^{\mathrm{H,H}})$ (Table 1, entry 5), from which the associated free energy changes $\Delta G_{\mathrm{connect}}^{\mathrm{H,L}k} = -RT\ln(f_{\mathrm{connect}}^{\mathrm{H,L}k})$ (Table 1, entry 4) and $\Delta E_{\mathrm{interaction}}^{\mathrm{H,H,L}k} = -RT\ln(u_{\mathrm{L}k}^{\mathrm{H,H}})$ (Table 1, entry 6) are deduced. We immediately notice that $\Delta G_{\mathrm{connect}}^{\mathrm{H,L2}} \ll \Delta G_{\mathrm{connect}}^{\mathrm{H,L1}} \leq \Delta G_{\mathrm{connect}}^{\mathrm{H,L3}}$, a trend resulting from the special ability of $[\mathrm{H}_n\mathbf{L2}]^{n+}$ for adopting the cis−cis conformation, in which the three adjacent nitrogen donor atoms contribute to the fixation of the entering protons. In line with straightforward electrostatic arguments, the fixation of a second proton to $[\mathrm{HL}k]^{+}$ to give $[\mathrm{H_2L}k]^{2+}$ (k = 1, 2) is anticooperative ($\Delta E_{\mathrm{interaction}}^{\mathrm{H,H,L1}} \approx \Delta E_{\mathrm{interaction}}^{\mathrm{H,H,L2}} \approx 7$ kJ/mol; allosteric cooperativity factor $\alpha < 1$; Table 1, entry 7).[28] Surprisingly, the reverse situation is found for **L3**, for which complexation of the second proton is driven to completion by a slightly positive cooperative process [$\Delta E_{\mathrm{interaction}}^{\mathrm{H,H,L3}} = -5.0(1.7)$ kJ/mol; allosteric cooperativity factor $\alpha > 1$; Table 1, entry 7]. Let us now rearrange the general form of the competition equilibrium (4) for **L2** and **L3**.

$$\frac{|[\mathrm{Eu}(\mathbf{L}k)^{3+}]|}{|[\mathrm{H}\mathbf{L}k^{+}]|} = \frac{\beta_{1,0,1}^{\mathrm{Eu,H},\mathbf{L}k}}{\beta_{0,1,1}^{\mathrm{Eu,H},\mathbf{L}k}}\frac{(|\mathrm{H_2O}|_{\mathrm{tot}} - |\mathrm{H_2O}|)}{K_{\mathrm{a}}^{1}|\mathrm{H_2O}|}$$

$$\leq 0.01 \Rightarrow \beta_{1,0,1}^{\mathrm{Eu,H},\mathbf{L}k} \leq \frac{0.01K_{\mathrm{a}}^{1} - |\mathrm{H_2O}|}{(|\mathrm{H_2O}|_{\mathrm{tot}} - |\mathrm{H_2O}|)}\beta_{0,1,1}^{\mathrm{Eu,H},\mathbf{L}k} \quad (14)$$

Because $\beta_{0,1,1}^{\mathrm{Eu,H,L2}} = \beta_{1,1}^{\mathrm{H,L2}}$ is 3 orders of magnitude larger than $\beta_{1,1}^{\mathrm{H,L3}}$ under the same experimental conditions, we deduce that **L2** is a much better candidate than **L3** for the formation of stable six-membered complexes with large labile cations.

Complexation of Ligand L2 with Li$^{\mathrm{I}}$, Mg$^{\mathrm{II}}$, Zn$^{\mathrm{II}}$, and Y$^{\mathrm{III}}$. Electrospray ionization mass spectrometry (ESI-MS) titrations of **L2** with $\mathrm{LiClO_4}$ or $\mathrm{Mg(ClO_4)_2}$ ($|\mathbf{L2}|_{\mathrm{tot}}$ = 0.5 mM in $\mathrm{CH_3CN/CHCl_3}$ (1:1); $|\mathbf{M}|_{\mathrm{tot}}/|\mathbf{L2}|_{\mathrm{tot}}$ = 0.1−100) mainly show the signal of the protonated ligand $[\mathrm{H}\mathbf{L2}]^{+}$ (m/z 311.5), together with weak peaks corresponding to $[\mathrm{Li}(\mathbf{L2})]^{+}$ (m/z 318.5), $[\mathrm{Li_2}(\mathbf{L2})(\mathrm{CH_3CN})_2]^{2+}$ (m/z 204.9), $[\mathrm{Mg}(\mathbf{L2})_2]^{2+}$ (m/z 323.5), and $[\mathrm{Mg}(\mathbf{L2})(\mathrm{ClO_4})]^{+}$ (m/z 434.0). Parallel ^{1}H NMR titrations performed in the same solvent mixture with $|\mathbf{L2}|_{\mathrm{tot}}$ = 7.5 mM show faint evolution of the spectra for Li$^{\mathrm{I}}$, where only a massive excess of Li$^{\mathrm{I}}$ produces some noticeable changes (Figure S16 in the SI). The larger electrostatic factor z^2/R = 5.56 eu/Å calculated for $\mathrm{Mg^{2+}}$ improves the interaction with the nitrogen donor atoms of **L2**,[29] and ^{1}H NMR titrations in the range $|\mathbf{Mg}|_{\mathrm{tot}}/|\mathbf{L2}|_{\mathrm{tot}}$ = 0.1−1.0 evidence upfield shifts for H2 and H3, which are diagnostic for the meridional tercoordination of the ligand around Mg$^{\mathrm{II}}$ (Figure S17 in the SI). The unfavorable intermediate dynamic exchange regime operating on the NMR time scale at 298 K with Mg$^{\mathrm{II}}$ prevents a quantitative analysis of the thermodynamic complexation process in these conditions. With Zn$^{\mathrm{II}}$, the lower energy of the empty metal-centered 4s orbitals favors covalent interactions with soft nitrogen donor ligands[6i] and ^{1}H NMR titrations of **L2** with $\mathrm{Zn(CF_3SO_3)_2}$ show the successive formation of $[\mathrm{Zn}(\mathbf{L2})_2]^{2+}$ and $[\mathrm{Zn}(\mathbf{L2})]^{2+}$, which are in slow exchange on the NMR time scale (Figure S18 in the SI). The thorough integration of the signals of the various protons belonging to the three species **L2**, $[\mathrm{Zn}(\mathbf{L2})_2]^{2+}$, and $[\mathrm{Zn}(\mathbf{L2})]^{2+}$ along the titration process provides fair estimations for the thermodynamic stability constants associated with eqs 15 and 16 (Figure 6a and Appendix 2 in the SI).

$$\mathrm{Zn^{2+}} + \mathbf{L2} \rightleftharpoons [\mathrm{Zn}(\mathbf{L2})]^{2+} \quad \log(\beta_{1,1}^{\mathrm{Zn,L2}}) = 3.7(3) \quad (15)$$

$$\mathrm{Zn^{2+}} + 2\mathbf{L2} \rightleftharpoons [\mathrm{Zn}(\mathbf{L2})_2]^{2+} \quad \log(\beta_{1,2}^{\mathrm{Zn,L2}}) = 5.3(2) \quad (16)$$

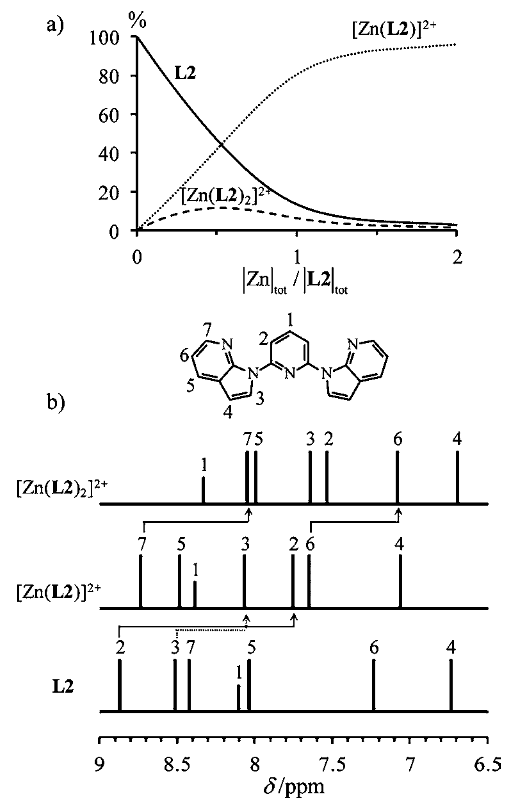

Figure 6. Computed (a) ligand distribution and (b) individual ^{1}H NMR spectra for **L2**, $[\mathrm{Zn}(\mathbf{L2})]^{2+}$, and $[\mathrm{Zn}(\mathbf{L2})_2]^{2+}$ [$\mathrm{CD_3CN/CDCl_3}$ (1:1); total ligand concentration 7.5 mm; 298 K].

The upfield shifts of H2 and H3 point to the usual meridional tercoordination (i.e., cis−cis conformation) of **L2** to Zn$^{\mathrm{II}}$ in the two complexes (Figure 6b and Table S1 in the SI) as substantiated by the molecular structure of $[\mathrm{Zn}(\mathbf{L2})(\mathrm{CF_3SO_3})_2]$ (**6**) deduced from X-ray diffraction studies (Figure 7 and Tables S18−S20 in the SI). The asymmetric unit in **6** contains two independent slightly different molecules A and B related by π−π-stacking interactions (Figure S19 in the SI). Because B-$[\mathrm{Zn}(\mathbf{L2})_2](\mathrm{CF_3SO_3})_2$ is less disordered, it will be

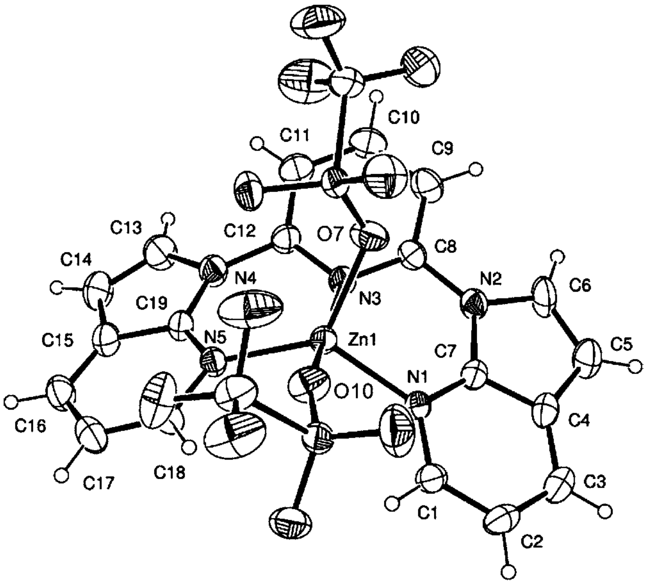

Figure 7. ORTEP view of **6** (complex B) observed in the crystal structure of **6** with an atomic numbering scheme. Thermal ellipsoids are represented at the 50% probability level.

considered for the discussion of the molecular structure (Figure 7).

In order to accommodate acceptable Zn−N bond distances in the 1.98−2.25 Å range (Table S19 in the SI), the bound ligand **L2** is severely twisted (intramolecular azaindole−pyridine interplanar angles = 25−28°; Table S20 in the SI), as was previously noticed for [Cu(**L2**)(NO_3)$_2$] (interplanar angle = 23.0°).[10] However, the overall helical twist found in the latter complex or in analogous palladium(II) and platinum(II) complexes[12,30,31] is replaced with a butterfly conformation in [Zn(**L2**)](CF_3SO_3)$_2$ (**6**; Figure S20 in the SI). This produces an unprecedented axially elongated pseudobipyramidal-trigonal arrangement of the five donor atoms about Zn^{II}, with N3 and O10 occupying the axial position and N1, N5, and O7 forming the trigonal basis (Figure 7). The nonplanarity of the polyaromatic backbone is characteristic for the tercoordination of the fused six-membered chelate rings **L2**[10,12] and **L3**[9,11] to the metal, which contrasts with the planar arrangement of the terpyridine ligand in [Zn(**L1**)Br_2] (twist angle < 1°).[31] The associated loss in aromaticity explains the low stability constants $\log(\beta_{1,1}^{\mathrm{Zn,L2}})$ = 3.7(3) (eq 15) observed for $[\mathrm{Zn}(\mathbf{L2})]^{2+}$, which is 4 orders of magnitude weaker than that reported for $[\mathrm{Zn}(\mathbf{L1})]^{2+}$ (water, ionic strength = 0).[6i] The fixation of a second ligand to give $[\mathrm{Zn}(\mathbf{L2})_2]^{2+}$ is almost statistical (vide infra), and the latter complex counts for less than 10% of the ligand speciation at millimolar concentrations (Figure 6a). We, however, note the considerable upfield shifts of the ^{1}H NMR signals of the terminal protons H6 and H7 on going from $[\mathrm{Zn}(\mathbf{L2})]^{2+}$ to $[\mathrm{Zn}(\mathbf{L2})_2]^{2+}$, a behavior diagnostic for their location in the shielding region of the second aromatic ligand bound to the same metal in pseudooctahedral bis-terdentate complexes.[32] Applying the thermodynamic site-binding model to eqs 15 and 16 gives eqs 17 and 18, from which the free energy of connection of Zn^{II} to the tridentate binding ligand **L2** [$\Delta G_{\mathrm{connect}}^{\mathrm{Zn,L2}} = -RT\ln(G_{\mathrm{connect}}^{\mathrm{Zn,L2}}) = -11.5(1.7)$ kJ/mol] can be estimated, together with a negligible anticooperative interligand interaction [$\Delta E_{\mathrm{Zn}}^{\mathrm{L2,L2}} = -RT\ln(u_{\mathrm{Zn}}^{\mathrm{L2,L2}}) = 0.7(2.7)$ kJ/mol; Figure S21 in the SI].

$$\beta_{1,1}^{\mathrm{Zn,L2}} = 48 f_{\mathrm{connect}}^{\mathrm{Zn,L2}} \quad (17)$$

$$\beta_{2,1}^{\mathrm{Zn,L2}} = 24 (f_{\mathrm{connect}}^{\mathrm{Zn,L2}})^2 u_{\mathrm{Zn}}^{\mathrm{L2,L2}} \quad (18)$$

Because $\Delta G_{\mathrm{connect}}^{\mathrm{Zn,L2}} \gg \Delta G_{\mathrm{connect}}^{\mathrm{H,L2}}$, competition with protonation is expected to be very severe, in line with the quantitative formation of $[\mathrm{H}\mathbf{L2}]^+$ upon the reaction of **L2** with triply charged Eu^{3+} in a wet solvent (Figure S2b in the SI). With

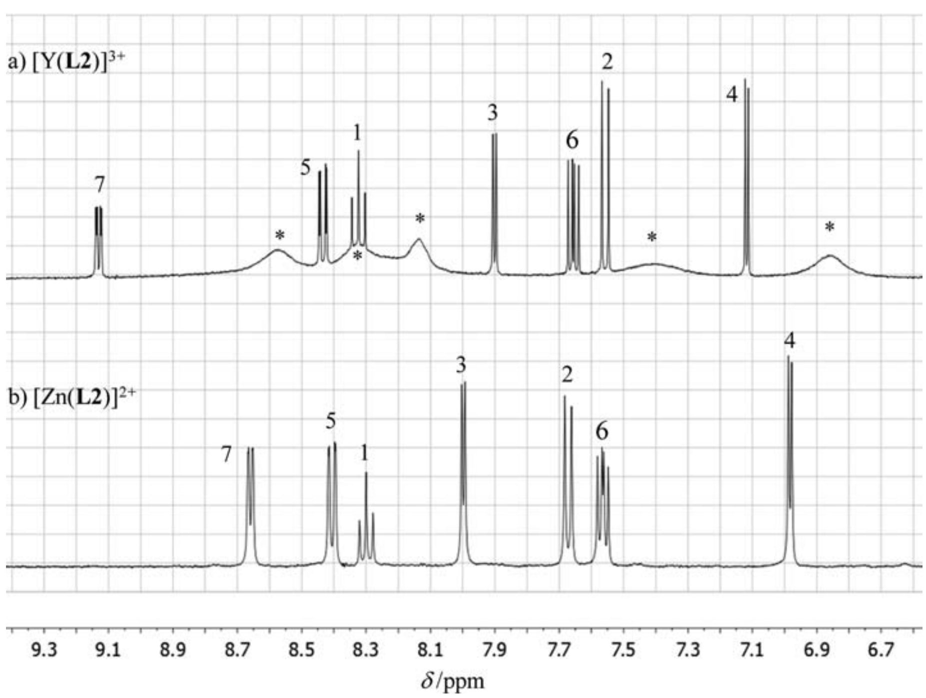

Figure 8. ^{1}H NMR spectra of (a) $[\mathrm{Y}(\mathbf{L2})]^{3+}$ (CD_2Cl_2) and (b) $[\mathrm{Zn}(\mathbf{L2})]^{2+}$ [CD_2Cl_2/CD_3CN (1:1)] at 298 K. Asterisks indicate residual signals of $[\mathrm{Y}(\mathbf{L2})_2]^{3+}$.

dx.doi.org/10.1021/ic301126y | Inorg. Chem. 2012, 51, 8567−8575

these thermodynamic results in mind, we decided to react **L2** (7.5 mM) with anhydrous YI_3 in dry CD_2Cl_2 in order to remove traces of competiting protons. Because of the minor solubility of YI_3 in this solvent, we are limited to $|YI_3|_{tot}/|\mathbf{L2}|_{tot} < 1.0$, but we undeniably observe the formation of $[Y(\mathbf{L2})]^{3+}$ as the major component in the mixture, together with the residual dynamically broadened upfield-shifted signals of $[Y(\mathbf{L2})_2]^{3+}$ (Figure 8a and Table S1 in the SI). The ^{1}H NMR spectrum recorded for $[Y(\mathbf{L2})]^{3+}$ closely matches that obtained for $[Zn(\mathbf{L2})]^{2+}$ (Figure 8b) and points to very similar conformations for the bound tridentate ligand around the metals. The noticeable 0.35 ppm downfield shift of H7 in $[Y(\mathbf{L2})]^{3+}$ confirms the larger positive charge born by Y^{III}.[17]

■ CONCLUSION

The insertion of an additional phenyl ring between the distal and central pyridine rings on going from **L1** (five-membered chelate ligand) to **L3** (six-membered chelate ligand) has only minor effects on the global thermodynamic of protonation in $CD_3CN/CDCl_3$, with both systems requiring a large excess of acids for their quantitative diprotonation at millimolar concentrations. The reluctance of **L3** for binding large lanthanide cations can be thus safely assigned to the weak affinity of this latter ligand for Eu^{III} ($\beta_{1,0,1}^{Eu,H,\mathbf{L3}} \ll \beta_{1,0,1}^{Eu,H,\mathbf{L1}}$). According to a geometrical point of view, the transformation of the obtuse isosceles triangle drawn by the three nitrogen donor atoms in the cis−cis conformation of $[H_2\mathbf{L1}]^{2+}$ into an acute isosceles triangle in $[H_2\mathbf{L3}]^{2+}$ supports the difficult incorporation of large cations by two fused six-membered chelate rings. The considerable affinity of **L2** for the entering proton contrasts with this picture ($\beta_{1,1}^{H,\mathbf{L2}} \gg \beta_{1,1}^{H,\mathbf{L1}}, \beta_{1,1}^{H,\mathbf{L3}}$), and **L2** indeed complexes larger labile cations Mg^{II}, Zn^{II}, and Y^{III} at millimolar concentrations. Although modest, the formation constants estimated for $[Zn(\mathbf{L2})_n]^{2+}$ are compatible with exploration of the selectivity induced by this novel class of neutral N-heterocyclic ligands along the 3d- and 4f-block series.

■ EXPERIMENTAL SECTION

Chemicals were purchased from Strem, Acros, Fluka AG, and Aldrich and used without further purification unless otherwise stated. The trifluoromethanesulfonate salt $Eu(CF_3SO_3)_3\cdot H_2O$ was prepared from the corresponding oxide (Aldrich, 99.99%).[33] $YI_3(THF)_{3.5}$ was isolated from the reaction of elemental iodine with powdered yttrium metal.[34] The ligands **L2**[7] and **L3**[8] were prepared according to literature procedures. We were, however, unable to reproduce the 80% yield reported for the Suzuki−Miyaura cross-coupling leading to **L3** (Appendix 3). Silica gel plates Merck $60F_{254}$ were used for thin layer chromatography, and Fluka silica gel 60 (0.04−0.063 mm) or Acros neutral activated alumina (0.050−0.200 mm) was used for preparative column chromatography.

Preparation of $[Zn(L2)](CF_3SO_3)_2$ (6). Stoichiometric amounts of **L2** (50 mg, 0.16 mmol) and $Zn(CF_3SO_3)_2$ (59.3 mg, 0.16 mmol) were reacted in acetonitrile/dichloromethane (1:1; 10 mL) at room temperature for 2 h. The solvent was evaporated, and the resulting white-off solid was dissolved in acetonitrile (3 mL). The slow diffusion of diethyl ether afforded X-ray-quality prisms of **6** (63.4 mg, 92.5 μmol, 56% yield). ^{1}H NMR [$CDCl_3/CD_3CN$ (1:1), 400 MHz]: δ 8.74 (dd, 2H, ^3J = 5.4 MHz, ^4J = 1.4 MHz), 8.49 (dd, 2H, ^3J = 7.9 MHz, ^4J = 1.5 MHz), 8.39 (t, 1H, ^3J = 5.4 MHz), 8.08 (d, 2H, ^3J = 4 MHz), 7.76 (d, 2H, ^3J = 8.3 MHz), 7.66 (dd, 2H, ^3J = 7.8 MHz, ^4J = 5.4 MHz), 7.07 (d, 2H, ^3J = 4 MHz). Elem anal. Calcd for $ZnC_{21}H_{13}N_5O_6S_2F_6$: C, 37.37; H, 1.94; N, 10.38. Found: C, 37.27; H, 2.05; N, 10.19.

Spectroscopic Measurements. ^{1}H and ^{13}C NMR spectra were recorded on a Bruker Avance 400 MHz spectrometer. Chemical shifts are given in ppm with respect to tetramethylsilane. In a typical ^{1}H NMR tiration experiment, 500 μL of a 7.5×10^{-3} M solution of ligand $\mathbf{L}k$ in $CD_3CN/CDCl_3$ (1:1) were reacted with successive aliquots of solutions of CF_3SO_3H, $LiClO_4$, $Mg(ClO_4)_2$, $Zn(CF_3SO_3)_2$, or $YI_3(THF)_{3.5}$ in the same solvent mixture. After each aliquot, the ^{1}H NMR spectrum was recorded at 298 K and the global chemical shift matrix was fitted to equilibria (5) and (6) by using *HypNMR-2008* software.[16] Pneumatically assisted electrospray (ESI-MS) mass spectra were recorded from 10^{-4} M solutions on an Applied Biosystems API 150EX LC/MS system equipped with a Turbo Ionspray source. Elemental analyses were performed by K. L. Buchwalder from the Microchemical Laboratory of the University of Geneva.

X-ray Crystallography. The crystal data, intensity measurements, and structure refinements for **1**−**4**, $[H_2\mathbf{L2}]I_2$ (**5**), and **6** were collected in Tables S2 and S18 (SI). All crystals were mounted on quartz fibers with protection oil. Cell dimensions and intensities were measured at 180 or 293 K on a Agilent Supernova diffractometer with mirror-monochromated Cu-Kα radiation (λ = 1.54184 Å). Data were corrected for Lorentz and polarization effects and for absorption. The structures were solved by direct methods (*SIR97*);[35] all other calculations were performed with *SHELX97*[36] systems and *ORTEP3*[37] programs. CCDC 853589−853592 (**1**−**4**) and CCDC 883807 and 883808 (**5** and **6**) contain the supplementary crystallographic data. The CIF files can be obtained free of charge via www.ccdc.cam.ac.uk/conts/retrieving.html (or from the Cambridge Crystallographic Data Centre, 12 Union Road, Cambridge CB2 1EZ, U.K.; fax (+44) 1223-336-033 or deposit@ccdc.cam.ac.uk).

■ ASSOCIATED CONTENT

Ⓢ Supporting Information

Derivation of eq 4 (Appendix 1), speciation for the zinc(II) complexes (Appendix 2), and experimental synthetic parts for **L2**, **L3**, and $YI_3(THF)_{3.5}$ (Appendix 3), tables of ^{1}H NMR chemical shifts, data crystal data, geometric parameters, bond distances, and bond angles, figures showing molecular structures with numbering schemes and crystal packing, symmetry numbers, and ^{1}H NMR titrations, and a CIF file for compounds **1**−**6**. This material is available free of charge via the Internet at http://pubs.acs.org.

■ AUTHOR INFORMATION

Corresponding Author

*E-mail: Claude.Piguet@unige.ch.

Notes

The authors declare no competing financial interest.

■ ACKNOWLEDGMENTS

Financial support from the Swiss National Science Foundation is gratefully acknowledged.

■ REFERENCES

(1) (a) Hancock, R. D. *J. Chem. Educ.* **1992**, *69*, 615−621. (b) Motekaitis, R. J.; Martell, A. E.; Hancock, R. D. *Coord. Chem. Rev.* **1994**, *133*, 39−65 and references cited therein.

(2) (a) Gan, X.-M.; Duesler, E. N.; Paine, R. T. *Inorg. Chem.* **2001**, *40*, 4420−4427. (b) Paine, R. T.; Tan, Y.-C.; Gan, X.-M. *Inorg. Chem.* **2001**, *40*, 7009−7013. (c) Huskowska, E.; Turowska-Tyrk, I.; Legendziewicz, J.; Riehl, J. P. *New J. Chem.* **2002**, *26*, 1461−1467. (d) Gan, X.; Rapko, B. M.; Duesler, E. N.; Binyamin, I.; Paine, R. T.; Hay, B. P. *Polyhedron* **2005**, *24*, 469−474. (e) Binyamin, I.; Pailloux, S.; Duesler, E. N.; Rapko, B. M.; Paine, R. T. *Inorg. Chem.* **2006**, *45*, 5886−5892. (f) Pailloux, S.; Shirima, C. E.; Ray, A. D.; Duesler, E. N.; Paine, R. T.; Klaehn, J. R.; McIlwain, M. E.; Hay, B. P. *Inorg. Chem.* **2009**, *48*, 3104−3113. (g) Eliseeva, S. V.; Pleshkov, D. N.; Lyssenko, K. A.; Lepnev, L. S.; Bünzli, J.-C. G.; Kuzmina, N. P. *Inorg. Chem.* **2011**, *50*, 5137−5144.

(3) (a) Laus, S.; Ruloff, R.; Toth, E.; Merbach, A. E. *Chem.—Eur. J.* **2003**, *9*, 3555−3566. (b) Polasek, M.; Rudovsky, J.; Hermann, P.; Lukes, I.; Vander Elst, L.; Muller, K. N. *Chem. Commun.* **2004**, 2602−2603. (c) Moore, E. G.; Samuel, A. P. S.; Raymond, K. N. *Acc. Chem. Res.* **2009**, *42*, 542−552 and references cited therein.
(4) (a) Wu, S. L.; Horrocks, W. deW. *J. Chem. Soc., Dalton Trans.* **1997**, 1497−1502. (b) Elhabiri, M.; Scopelliti, R.; Bünzli, J.-C. G.; Piguet, C. *J. Am. Chem. Soc.* **1999**, *121*, 10747−10762. (c) Datta, A.; Raymond, K. N. *Acc. Chem. Res.* **2009**, *42*, 938−947 and references cited therein. (d) Tei, L.; Baranyai, Z.; Brücher, E.; Cassino, C.; Demicheli, F.; Masciocchi, N.; Giovenzana, G. B.; Botta, M. *Inorg. Chem.* **2010**, *49*, 616−625.
(5) (a) Semenova, L. J.; Skelton, B. W.; White, A. H. *Aust. J. Chem.* **1999**, *52*, 551−569. (b) Semenova, L. J.; White, A. H. *Aust. J. Chem.* **1999**, *52*, 571−600. (c) van Staveren, D. R.; van Albada, G. A.; Haasnoot, J. G.; Kooijman, H.; Lanfredi, A. M. M.; Neuwenhuizen, P. J.; Spek, A. L.; Ugozzoli, F.; Weyermüller, T.; Reedijk, J. *Inorg. Chim. Acta* **2001**, *315*, 163−171. (d) Puntus, L. N.; Lyssenko, K. A.; Pekareva, I. S.; Bünzli, J.-C. G. *J. Phys. Chem. B* **2009**, *113*, 9265−9277. (e) Kubicek, V.; Hamplova, A.; Maribé, L.; Mameri, S.; Ziessel, R.; Toth, E.; Charbonnière, L. J. *Dalton Trans.* **2009**, 9466−9474.
(6) (a) Chapman, R. D.; Loda, R. T.; Riehl, J. P.; Schwartz, R. W. *Inorg. Chem.* **1984**, *23*, 1652−1657. (b) Kepert, C. J.; Lu, W.-M.; Semenova, L. J.; Skelton, B. W.; White, A. H. *Aust. J. Chem.* **1999**, *52*, 481−496. (c) Semenova, L. J.; White, A. H. *Aust. J. Chem.* **1999**, *52*, 507−517. (d) Semenova, L. J.; White, A. H. *Aust. J. Chem.* **1999**, *52*, 539−550. (e) Drew, M. G. B.; Iveson, P. B.; Hudson, M. J.; Liljenzin, J. O.; Spjuth, L.; Cordier, P.-Y.; Enarsson, A.; Hill, C.; Madic, C. *J. Chem. Soc., Dalton Trans.* **2000**, 821−830. (f) Drew, M. G. B.; Hudson, M. J.; Iveson, P. B.; Madic, C.; Russel, M. L. *J. Chem. Soc., Dalton Trans.* **2000**, 2711−2720. (g) Mürner, H.-R.; Chassat, E.; Thummel, R. P.; Bünzli, J.-C. G. *J. Chem. Soc., Dalton Trans.* **2000**, 2809−2816. (h) Petit, L.; Daul, C.; Adamo, C.; Maldivi, P. *New J. Chem.* **2007**, *31*, 1738−1745. (i) Hamilton, J. M.; Anhorn, M. J.; Oscarson, K. A.; Reibenspies, J. H.; Hancock, R. D. *Inorg. Chem.* **2011**, *50*, 2764−2770.
(7) Wu, Q.; Lavigne, J. A.; Tao, Y.; D'Iorio, D.; Wang, S. *Chem. Mater.* **2001**, *13*, 71−77.
(8) Jäger, M.; Eriksson, L.; Bergquist, J.; Johansson, O. *J. Org. Chem.* **2007**, *72*, 10227−10230.
(9) Berggren, G.; Huang, P.; Eriksson, L.; Anderlund, M. F. *Appl. Magn. Reson.* **2009**, *36*, 9−24.
(10) Collins, S. N.; Taylor, S.; Krause, J. A.; Connick, W. B. *Acta Crystallogr.* **2007**, *C63*, m436−m439.
(11) (a) Abrahamson, M.; Jäger, M.; Osterman, T.; Eriksson, L.; Persson, P.; Becker, H.-C.; Johansson, O.; Hammarström, L. *J. Am. Chem. Soc.* **2006**, *126*, 12616−12617. (b) Jäger, M.; Kumar, R. J.; Göns, H.; Bergquist, J.; Johansson, O. *Inorg. Chem.* **2009**, *48*, 3228−3238. (c) Sharma, S.; Lombeck, F.; Eriksson, L.; Johansson, O. *Chem.—Eur. J.* **2010**, *16*, 7078−7081. (d) Hammarström, L.; Johansson, O. *Coord. Chem. Rev.* **2010**, *254*, 2545−2559.
(12) Garner, K. L.; Parkes, L. F.; Piper, J. D.; Williams, J. A. G. *Inorg. Chem.* **2010**, *49*, 476−487.
(13) Baes, C. F. J.; Mesmer, R. E. *Hydrolysis of Cations*; Wiley-Interscience: New York, 1976; Chapter 7, p 129.
(14) Hamilton, J. M.; Whitehead, J. R.; Williams, N. J.; Ojaimi, M. E.; Thummel, R. P.; Hancock, R. D. *Inorg. Chem.* **2011**, *50*, 3785−3790.
(15) (a) El-Gahami, M. A.; Ibrahim, S. A.; Fouad, D. M.; Hammam, A. M. *J. Chem. Eng. Data* **2003**, *48*, 29−31. (b) Marie, C.; Miguirditchian, M.; Guillaumont, D.; Tosseng, A.; Berthon, C.; Guilbaud, P.; Duvail, M.; Bisson, J.; Guillaneux, D.; Pipelier, M.; Dubreuil, D. *Inorg. Chem.* **2011**, *50*, 6557−6566.
(16) *HypNMR-2008* software: (a) Frassineti, C.; Ghelli, S.; Gans, P.; Sabatini, A.; Moruzzi, M. S.; Vacca, A. *Anal. Biochem.* **1995**, *231*, 374−382. (b) Frassineti, C.; Alderighi, L.; Gans, P.; Sabatini, A.; Vacca, A.; Ghelli, S. *Bioanal. Chem.* **2003**, *376*, 1041−1052.
(17) Lavallee, D. K.; Baughman, M. D.; Phillips, M. D. *J. Am. Chem. Soc.* **1977**, *99*, 718−724.
(18) (a) Nakamoto, K. *J. Phys. Chem.* **1960**, *64*, 1420−1425. (b) Bessel, C. A.; See, R. F.; Jameson, D. L.; Churchill, M. R.; Takeuchi, K. J. *J. Chem. Soc., Dalton Trans.* **1992**, 3223−3228. (c) Bowes, K. F.; Clark, I. P.; Cole, J. M.; Gourlay, M.; Griffin, M. E.; Mahon, M. F.; Ooi, L.; Parker, A. W.; Raithby, P. R.; Sparkesc, H. A.; Towrie, M. *Cryst. Eng. Commun.* **2005**, *7*, 269−275.
(19) Göller, A. H.; Grummt, U.-W. *Chem. Phys. Lett.* **2002**, *354*, 233−242.
(20) Hergold-Brundic, A.; Popovic, Z.; Matkovic-Calogovoc, D. *Acta Crystallogr.* **1996**, *C52*, 3154−3157.
(21) (a) Kepert, C. J.; Skelton, B. W.; White, A. H. *Aust. J. Chem.* **1994**, *47*, 391−396. (b) Drew, M. G. B.; Hudson, M. J.; Iveson, P. B.; Russell, M. L.; Lilijenzin, J.-O.; Skalberg, M.; Spjuth, L.; Madic, C. *J. Chem. Soc., Dalton Trans.* **1998**, 2973−2980. (c) Berthon, C.; Grigoriev, M. S. *Acta Crystallogr.* **2005**, *E61*, o1216−o1217.
(22) Bazzicalupi, C.; Bencini, A.; Bianchi, A.; Danesi, A.; Faggi, E.; Giorgi, C.; Santarelli, S.; Valtancoli, B. *Coord. Chem. Rev.* **2008**, *252*, 1052−1068.
(23) For a forced coplanar trans−trans arrangement of the three aromatic rings in **L3**, we calculate a H(py)···N(quinoline) contact distance of 1.94 Å, a value much shorter than the sum of the van der Waals radii (1.46 + 1.06 = 2.52 Å). Bondi, A. *J. Phys. Chem.* **1964**, *68*, 441−451.
(24) All hydrogen atoms were observed from the difference Fourier map and refined without constraints except for **4**, where restraints on the bond lengths and bond angles were applied for aromatic hydrogen atoms connected to carbon atoms, but the additional hydrogen atom bound to nitrogen atom was freely refined.
(25) The nature of the hydrogen-bound counteranions has only a minor effect on the conformation of the protonated cations, as exemplified by the almost superimposable molecular structures of $[H\mathbf{L2}]^+$ in **1** and $[H\mathbf{L2}](FeCl_4)$[10] (Figure S11 in the SI) and for $[H_2\mathbf{L2}]^{2+}$ in **2** and $[H_2\mathbf{L2}]I_2$ (**5**; Figure S12 in the SI).
(26) (a) Hamacek, J.; Borkovec, M.; Piguet, C. *Chem.—Eur. J.* **2005**, *11*, 5227−5237. (b) Hamacek, J.; Borkovec, M.; Piguet, C. *Chem.—Eur. J.* **2005**, *11*, 5217−5226. (c) Hamacek, J.; Borkovec, M.; Piguet, C. *Dalton Trans.* **2006**, 1473−1490. (d) Piguet, C. *Chem. Commun.* **2010**, *46*, 6209−6231.
(27) Ercolani, G.; Piguet, C.; Borkovec, M.; Hamacek, J. *J. Phys. Chem. B* **2007**, *111*, 12195−12203.
(28) Ercolani, G.; Schiaffino, L. *Angew. Chem., Int. Ed.* **2011**, *50*, 1762−1768.
(29) Wulfsberg, G. *Inorganic Chemistry*; University Science Books: Sausalito, CA, 2000; Chapter 2.
(30) Song, D.; Wu, Q.; Hook, A.; Kozin, I.; Wang, S. *Organometallics* **2001**, *20*, 4683−4689.
(31) Zhao, Q.-L.; Li, G.-P. *Acta Crystallogr.* **2009**, *E65*, m693.
(32) (a) Piguet, C.; Bochet, C. G.; Williams, A. F. *Helv. Chim. Acta* **1993**, *76*, 372−384. (b) Constable, E. C.; Baum, G.; Bill, E.; Dyson, R.; van Eldik, R.; Fenske, D.; Kaderli, S.; Morris, D.; Neubrand, A.; Neuburger, M.; Smith, D. R.; Wieghardt, K.; Zehnder, M.; Zuberbühler, A. D. *Chem.—Eur. J.* **1999**, *5*, 498−508.
(33) Desreux, J. F. In *Lanthanide Probes in Life, Chemical and Earth Sciences*; Bünzli, J.-C. G., Choppin, G. R., Eds.; Elsevier: Amsterdam, The Netherlands, 1989; Chapter 2, p 43.
(34) Izod, K.; Liddle, S. T.; Clegg, W. *Inorg. Chem.* **2004**, *43*, 214−218.
(35) Altomare, A.; Burla, M. C.; Camalli, M.; Cascarano, G.; Giacovazzo, C.; Guagliardi, A.; Moliterni, G.; Polidori, G.; Spagna, R. *J. Appl. Crystallogr.* **1999**, *32*, 115−119.
(36) Sheldrick, G. M. *SHELXL97: Program for the Solution and Refinement of Crystal Structures*; University of Göttingen: Göttingen, Germany, 1997.
(37) *ORTEP3* for Windows: Farrugia, L. J. *J. Appl. Crystallogr.* **1997**, *30*, 565.